



# Total nodule number as an independent prognostic factor in resected stage III non-small cell lung cancer: a deep learning-powered study

Xiuyuan Chen<sup>1#</sup>, Qingyi Qi<sup>2#</sup>, Zewen Sun<sup>1#</sup>, Dawei Wang<sup>3</sup>, Jinlong Sun<sup>3</sup>, Weixiong Tan<sup>3</sup>, Xianping Liu<sup>1</sup>, Taorui Liu<sup>1</sup>, Nan Hong<sup>2</sup>, Fan Yang<sup>1</sup>

<sup>1</sup>Department of Thoracic Surgery, Peking University People's Hospital, Beijing, China; <sup>2</sup>Department of Radiology, Peking University People's Hospital, Beijing, China; <sup>3</sup>Institute of Advanced Research, Beijing Infervision Technology Co., Ltd., Beijing, China

**Contributions:** (I) Conception and design: X Chen, F Yang; (II) Administrative support: N Hong, F Yang; (III) Provision of study materials or patients: D Wang, J Sun, W Tan; (IV) Collection and assembly of data: Q Qi, X Liu, T Liu; (V) Data analysis and interpretation: Z Sun, X Chen; (VI) Manuscript writing: All authors; (VII) Final approval of manuscript: All authors.

<sup>#</sup>These authors contributed equally to this work.

**Correspondence to:** Nan Hong. Department of Radiology, Peking University People's Hospital, 11 Xizhimen South Street, Beijing 100044, China. Email: hongnan@bjmu.edu.cn; Fan Yang. Department of Thoracic Surgery, Peking University People's Hospital, 11 Xizhimen South Street, Beijing 100044, China. Email: yangfan@pkuph.edu.cn.

**Background:** Almost every patient with lung cancer has multiple pulmonary nodules; however, the significance of nodule multiplicity in locally advanced non-small cell lung cancer (NSCLC) remains unclear.

**Methods:** We identified patients who had undergone surgical resection for stage I–III NSCLC at the Peking University People's Hospital from 2005 to 2018 for whom preoperative chest computed tomography (CT) scans were available. Deep learning-based artificial intelligence (AI) algorithms using convolutional neural networks (CNN) were applied to detect and classify pulmonary nodules (PNs). Maximally selected log-rank statistics were used to determine the optimal cutoff value of the total nodule number (TNN) for predicting survival.

**Results:** A total of 33,410 PNs were detected by AI among the 2,126 participants. The median TNN detected per person was 12 [interquartile range (IQR) 7–20]. It was revealed that AI-detected TNN (analyzed as a continuous variable) was an independent prognostic factor for both recurrence-free survival (RFS) [hazard ratio (HR) 1.012, 95% confidence interval (CI): 1.002 to 1.022,  $P=0.021$ ] and overall survival (OS) (HR 1.013, 95% CI: 1.002 to 1.025,  $P=0.021$ ) in multivariate analyses of the stage III cohort. In contrast, AI-detected TNN was not significantly associated with survival in the stage I and II cohorts. In a survival tree analysis, rather than using traditional IIIA and IIIB classifications, the model grouped cases according to AI-detected TNN (lower *vs.* higher: log-rank  $P<0.001$ ), which led to a more effective determination of survival rates in the stage III cohort.

**Conclusions:** The AI-detected TNN is significantly associated with survival rates in patients with surgically resected stage III NSCLC. A lower TNN detected on preoperative CT scans indicates a better prognosis for patients who have undergone complete surgical resection.

**Keywords:** Nodule number; non-small cell lung cancer (NSCLC); prognosis; artificial intelligence; multiple pulmonary nodules

Submitted Jun 22, 2021. Accepted for publication Nov 02, 2021.

doi: 10.21037/atm-21-3231

**View this article at:** <https://dx.doi.org/10.21037/atm-21-3231>

## Introduction

Lung cancer is a leading cause of cancer-related death worldwide (1). As early detection of cancer is important for decreasing mortality, multiple randomized trials and guidelines recommend lung cancer screening using low-dose computed tomography (LDCT) for high-risk individuals (2-7). With the adoption of LDCT for lung cancer screening, the number of chest CT scans has increased dramatically each year (8). To address the repetitive and onerous task of dealing with images that are mostly normal, computer-aided detection/diagnosis (CAD), which could perform the task consistently and tirelessly, has become extremely appealing (9).

Since 2002, CAD, supported by machine learning techniques, has been utilized to detect pulmonary nodules (PNs) (10). Although standardized CAD systems have been shown to improve diagnostic accuracy, few have been implemented in actual clinical practice due to their high dependence on image processing and false positive rates (11,12). In recent years, deep learning-based AI algorithms using convolutional neural networks (CNNs) have attracted considerable attention in the area of machine learning. The key advantage that CNNs have over conventional CAD techniques is their ability to self-learn previously unknown features, maximizing classification accuracy with limited direct supervision (13). The use of CNNs has led to a significant reduction in false positives in PN detection, recognition, segmentation, and classification (14-19), thus laying the foundation for the extensive clinical application of deep learning-based AI algorithms. The first deep learning-based AI algorithm for PN detection approved by the United States Food and Drug Administration (FDA) was used to guarantee PN detection performance in this study. Compared with AI algorithms reported in proof-of-concept studies, its robustness and generalizability have been widely validated in multiple medical centers and proven valuable in enhancing imaging report standardization and improving clinical workflow (20-22).

The key issue in the management of incidental PNs detected on CT images is to differentiate between benign and malignant nodules. Radiological features, such as larger nodule size, upper lobe location, marginal spiculation, and faster growth rate are generally considered risk factors for malignancy (23-28). These principles mainly focus on the assessment of the largest or most suspicious nodule. However, although approximately 50% of the patients with detected PNs have multiple nodules (29), nodule multiplicity, which is a potential indicator for malignancy,

is commonly overlooked. Only limited data concerning the relationship between TNN and lung cancer probability are available. In the Pan-Canadian Early Detection of Lung Cancer Study (PanCan) and the British Columbia Cancer Agency (BCCA) cancer screening trials, lower TNN was associated with an increased risk of lung cancer (23). However, another study analyzing patients from the Dutch-Belgian Lung Cancer Screening trial (NELSON) showed that the risk of lung cancer increased as the TNN rose from 1 to 4 but decreased in patients with 5 or more nodules (29).

The results of the abovementioned screening trials indicated that TNN was either negatively or not significantly associated with lung cancer probability, which might reflect a low incidence of multiple malignancies in the screening population (30). However, for patients with a high pretest probability of malignancy, it remains unknown whether TNN plays a role in (I) determining lung cancer probability with multiple pulmonary sites of involvement, (II) distinguishing multiple primary lung cancers (MPLC) from intrapulmonary metastasis (IPM), and (III) prognosis. This study aimed to calculate the TNN detected on preoperative CT images using a CNN-based AI algorithm and to deeply explore the relationship between AI-detected TNN and survival outcomes in patients with resectable stage I-III NSCLC. We report the following article in accordance with the Transparent Reporting of a multivariable prediction model for Individual Prognosis or Diagnosis (TRIPOD) statement checklist (available at <https://atm.amegroups.com/article/view/10.21037/atm-21-3231/rc>).

## Methods

### Patients

We retrospectively reviewed the medical records of patients pathologically diagnosed with stage I-III NSCLC [according to the 8<sup>th</sup> edition of the American Joint Committee on Cancer (AJCC) prognostic group] who had undergone surgical resection at the Department of Thoracic Surgery at the Peking University People's Hospital from October 2005 to December 2018. Only patients who received a preoperative chest CT scan within 90 days prior to surgery at the institution were included. Patients were excluded if 1 or more of the following conditions were met: (I) had already received neoadjuvant therapy, (II) surgical margin was positive, (III) perioperative death occurred within 30 days, or (IV) the follow-up information was inadequate.

Routine follow-up after the surgical intervention included an outpatient department visit every 3 months for the first 2 years and at 6-month intervals thereafter. For patients who failed to present at the clinic, follow-up information was collected via telephone call. We diagnosed recurrence based on physical and imaging examinations and confirmed the diagnosis histologically when clinically feasible. Secondary primary lung cancer was differentiated from intrapulmonary metastases using either the Martini-Melamed criteria or a comprehensive histological assessment (31).

### *AI-powered PN detection*

InferRead CT Lung (<https://global.infervision.com/product/30.html>), a widely used deep learning-based AI algorithm developed by InferVision (Beijing, China), was applied for PN detection in this study, and only the patient's last chest CT scan before surgery was used. First, PNs were detected by the AI algorithm, and the TNN was calculated accordingly. Next, PNs were classified according to their lobar distribution (left lower lobe, left upper lobe, right lower lobe, right middle lobe, and right upper lobe), location [same lobe as the primary tumor (same-lobe), ipsilateral lobe different from the primary tumor (same-side), and contralateral lobe (other-side)], and type [solid nodule, mixed ground-glass nodule (m-GGN), pure ground-glass nodule (p-GGN), calcific nodule, and periferfissural nodule]. In addition, solid and subsolid (m-GGN and p-GGN) nodules were categorized based on their size.

### *Statistical analysis*

Continuous variables were presented as a median with an interquartile range (IQR) and were analyzed using Wilcoxon's rank-sum test and one-way analysis of variance (ANOVA). Categorical variables were presented as frequencies and percentages. Survival curves were compared using the Kaplan-Meier method with a log-rank test, and Cox proportional hazards models were constructed to determine the independent prognostic factors.

In the stage III cohort, maximally selected log-rank statistics were used to determine the optimal nodule number cutoff value for predicting OS. Patients were then categorized into lower- and higher-nodule number groups according to the estimated cutoff value. Furthermore, a least absolute shrinkage and selection operator (LASSO)-based Cox regression model with cross-validation was used to select the most useful prognostic features among all categories of the

AI-detected nodule numbers. Finally, survival tree analysis was conducted to generate a tree-based model for survival data using log-rank test statistics for recursive partitioning.

All the statistical analyses were executed using R version 4.0.0 for Windows (R Foundation for Statistical Computing, Vienna, Austria). All the statistical tests were 2-sided, and P values of 0.05 or less were considered statistically significant.

### *Ethical statement*

The study was conducted in accordance with the Declaration of Helsinki (as revised in 2013). The study involving human participants was reviewed and approved by the Institutional Review Board of Peking University People's Hospital (2020PHB385-01). Individual consent for this retrospective analysis was waived.

## **Results**

### *Characteristics of participants and nodules*

A total of 2,126 patients who underwent surgical resection for stage I–III NSCLC and had accessible preoperative chest CT scans were included in this study. The median follow-up time was 33 months (IQR, 21 to 48). The demographic and clinicopathological characteristics of the patients are summarized in *Table 1*.

The framework of the deep learning-powered PN detection algorithm and an example of 3-dimensional (3D) reconstruction of the AI-detected nodules are shown in *Figure 1A,1B*. A total of 33,410 PNs were detected in the 2,126 patients. The features of these AI-detected nodules are provided in *Table 2*. The distributions of AI-detected TNN, solid nodule number, and subsolid nodule number per person were all positively skewed, and the medians of these 3 factors were 12 (IQR, 7 to 20), 6 (IQR, 3 to 10), and 3 (IQR, 1 to 6), respectively (*Figure 2A-2C*).

When considering discrepancies in nodule numbers among the different stages, we found that there was no statistically significant difference between the mean TNNs (one-way ANOVA  $P=0.655$ ). However, the mean solid nodule numbers were significantly higher in participants with stage II and III, while the mean subsolid nodule numbers were higher in those with stage I (both  $P<0.001$ , *Figure 2D-2F*). Moreover, patients with late-stage cancer tended to have more solid nodules with greater size (*Figure S1*).

**Table 1** Characteristics of the participant cohort (N=2,126)

Variables	Value
Age (years)	
Median [IQR]	61 [54–68]
Gender	
Male	998 (46.9%)
Female	1,128 (53.1%)
Smoking history	
No	1,456 (68.5%)
Yes	670 (31.5%)
Comorbidity	
No	850 (40.0%)
Yes	1,276 (60.0%)
Surgical approach	
VATS	1,997 (93.9%)
VATS converted to open	61 (2.9%)
Open	68 (3.2%)
Surgical procedure	
Sublobar resection	636 (29.9%)
Lobectomy	1,419 (66.8%)
Sleeve lobectomy	39 (1.8%)
Pneumonectomy	32 (1.5%)
Histologic type	
Adenocarcinoma	1,780 (83.7%)
Squamous cell carcinoma	280 (13.2%)
Others	66 (3.1%)
Pathologic T stage	
T1	1,383 (65.1%)
T2	579 (27.2%)
T3	115 (5.4%)
T4	49 (2.3%)
Pathologic N stage	
N0	1,765 (83.0%)
N1	145 (6.8%)
N2	216 (10.2%)

**Table 1** (continued)**Table 1** (continued)

Variables	Value
AJCC stage (8th edition)	
IA1	499 (23.5%)
IA2	515 (24.2%)
IA3	265 (12.5%)
IB	347 (16.3%)
IIA	53 (2.5%)
IIB	184 (8.7%)
IIIA	213 (10.0%)
IIIB	50 (2.3%)
Complications	
No	2,038 (95.9%)
Yes	88 (4.1%)
Adjuvant therapy	
No	1,294 (60.9%)
Yes	445 (20.9%)
Unknown	387 (18.2%)

IQR, interquartile range; VATS, video-assisted thoracoscopic surgery; AJCC, American Joint Committee on Cancer.

### Survival analyses

We analyzed the survival of participants by stage according to the 8<sup>th</sup> edition of the AJCC prognostic group (Figure 3A,3B). The differences in both recurrence-free survival (RFS) and overall survival (OS) between any 2 stages were statistically significant (pairwise comparison  $P < 0.001$ ). Cox proportional hazards models were then built to determine the prognostic factors of the entire cohort (Table S1). The TNN was not an independent prognostic factor for either RFS (HR 1.006, 95% CI: 0.999 to 1.012,  $P = 0.080$ ) or OS (HR 1.002, 95% CI: 0.995 to 1.009,  $P = 0.590$ ) after adjusting for clinicopathological variables.

Subgroup analyses stratified by stage showed that the TNN was not significantly associated with survival for patients with stage I (RFS: HR 1.010, 95% CI: 0.998 to 1.022,  $P = 0.102$ ; OS: HR 1.003, 95% CI: 0.989 to 1.017,  $P = 0.689$ ) and stage II cancer (RFS: HR 1.000, 95% CI: 0.988 to 1.013,  $P = 0.973$ ; OS: HR 1.000, 95% CI: 0.989 to 1.012,  $P = 0.965$ ). However, in the stage III cohort, lower TNN was independently associated with improved survival in multivariate analyses (RFS: HR 1.012,

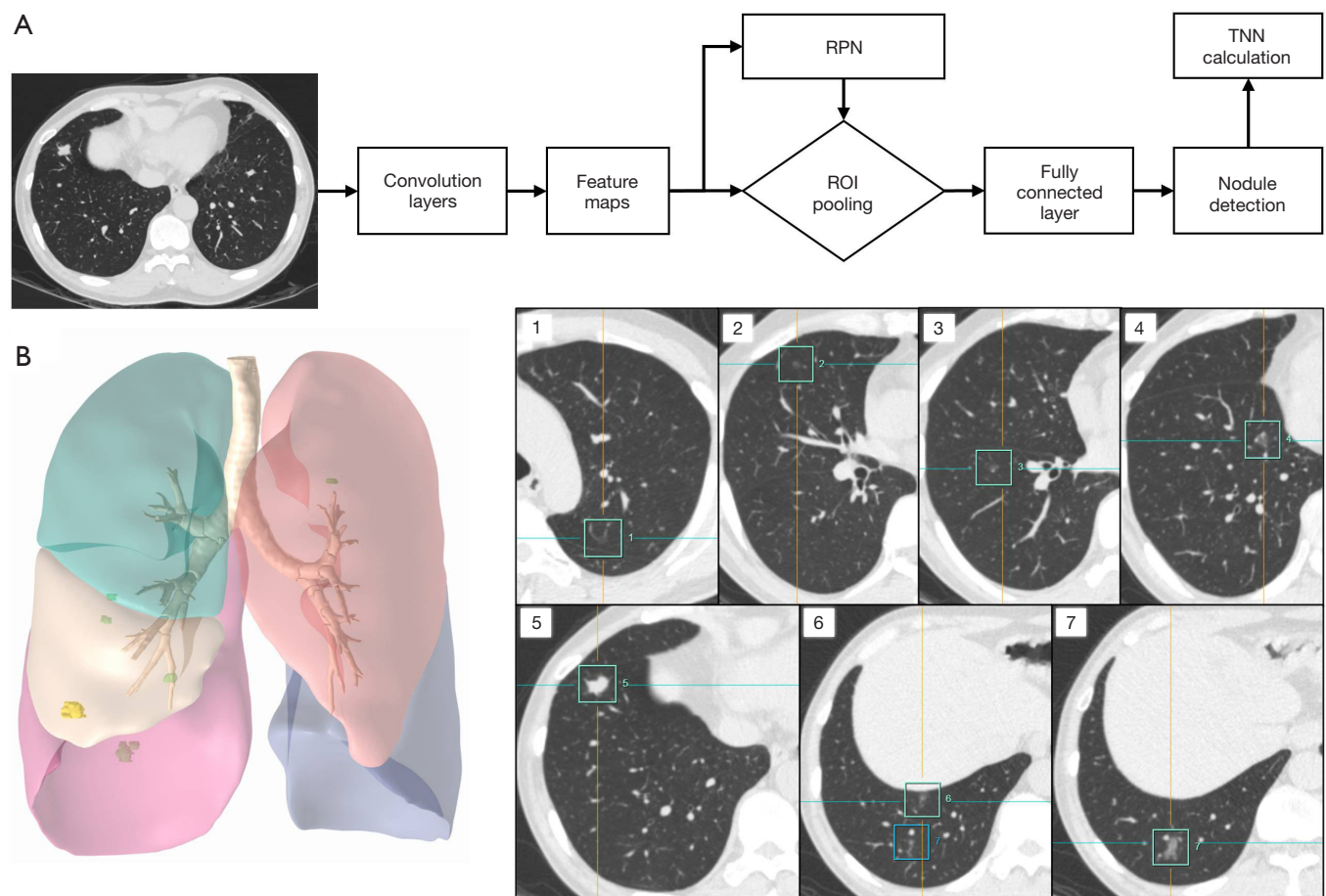


**Figure 1** The framework of the deep learning-powered pulmonary nodule detection algorithm and an example of the three-dimensional (3D) reconstruction of AI-detected nodules with corresponding CT images under the lung window setting. (A) Feature maps were extracted using CNN. An RPN was used to obtain potential regions from the extracted features. After ROI pooling and fully connected layers, nodules were detected with rectangular proposals. (B) Seven nodules were detected using the AI algorithm, including 1 solid nodule (#5), 2 mixed GGNs (#4, #7), and 4 pure GGNs (#1, #2, #3, #6). AI, artificial intelligence; RPN, regional proposal network; ROI, region of interest; TNN, total nodule number; CNN, convolutional neural network; GGN, ground-glass nodule.

95% CI: 1.002 to 1.022,  $P=0.021$ ; OS: HR 1.013, 95% CI: 1.002 to 1.025,  $P=0.021$ ) (Tables 3,4).

### Exploratory analyses in the stage III cohort

To further evaluate the prognostic effect of the AI-detected TNN, we used maximally selected log-rank statistics to categorize patients into lower- and higher-TNN groups. The optimal cutoff value of 8 was selected (Figure S2). Participants with a lower TNN ( $\leq 8$ ) had significantly improved OS (log-rank  $P<0.001$ , Figure 4A) compared with those with a higher TNN ( $>8$ ). Lower TNN was also an independent favorable predictor for OS in multivariate

analyses (HR 2.348, 95% CI: 1.351 to 4.082,  $P=0.002$ ).

To assess which of the components were associated with survival, we classified AI-detected nodules into different categories. When analyzed as continuous variables, the numbers of upper-lobe nodule (HR 1.028, 95% CI: 1.008 to 1.049,  $P=0.006$ ), same-side nodule (HR 1.032, 95% CI: 1.001 to 1.064,  $P=0.046$ ), other-side nodule (HR 1.020, 95% CI: 1.001 to 1.039,  $P=0.040$ ), solid nodule (HR 1.020, 95% CI: 1.004 to 1.036,  $P=0.012$ ), and even solid nodule at small size ( $\leq 6$  mm) (HR 1.027, 95% CI: 1.007 to 1.047,  $P=0.008$ ) were independently associated with OS in multivariate analyses. However, none of the numbers of the middle/lower-lobe nodule (HR 1.016, 95%

**Table 2** Characteristics of AI-detected pulmonary nodules (N=33,410)

Features	Value
Total nodule number, per person	
Median [IQR]	12 [7–20]
Lobar distribution	
Left lower lobe nodule	6,630 (19.9%)
Left upper lobe nodule	7,934 (23.7%)
Right lower lobe nodule	6,631 (19.9%)
Right middle lobe nodule	2,680 (8.0%)
Right upper lobe nodule	9,535 (28.5%)
Nodule location	
Same-lobe nodule	9,039 (27.0%)
Same-side nodule	9,114 (27.3%)
Other-side nodule	15,257 (45.7%)
Nodule type	
Solid nodule	17,790 (53.2%)
Mixed ground glass nodule	1,616 (4.8%)
Pure ground glass nodule	10,276 (30.8%)
Calcific nodule	2,799 (8.4%)
Perifissural nodule	929 (2.8%)
Solid nodule size	
≤6 mm	13,745 (77.2%)
>6 mm & ≤8 mm	1,487 (8.4%)
>8 mm	2,558 (14.4%)
Mixed ground glass nodule size	
≤6 mm	273 (16.9%)
>6 mm	1,343 (83.1%)
Pure ground glass nodule size	
≤6 mm	6,675 (65.0%)
>6 mm	3,601 (35.0%)

AI, artificial intelligence; IQR, interquartile range.

CI: 0.994 to 1.039,  $P=0.153$ ), same-lobe nodule (HR 1.021, 95% CI: 0.986 to 1.056,  $P=0.246$ ), m-GGN (HR 1.104, 95% CI: 0.885 to 1.376,  $P=0.381$ ), p-GGN (HR 1.015, 95% CI: 0.976 to 1.056,  $P=0.462$ ), calcific nodule (HR 1.021, 95% CI: 0.975 to 1.068,  $P=0.384$ ), or perifissural nodule (HR 1.007, 95% CI: 0.792 to 1.279,  $P=0.957$ ) were

significantly associated with survival. The 5 independent prognostic nodule numbers were then set as binary variables according to their optimal cutoff values. Similarly, participants with lower nodule numbers had significantly improved OS compared with those with higher nodule numbers (Figure 4B–4F).

Finally, to evaluate which of the components contributed most to prognosis, a LASSO-based Cox regression model incorporating both clinicopathological features and all categories of AI-detected nodule numbers (as continuous variables) was built (Figure S3). The resulting 7 features with a nonzero coefficient were as follows: age (0.021), smoking history (0.106), surgical approach (0.669), adjuvant therapy status (−0.389), IIIA/IIIB classification (0.095), upper-lobe nodule number (0.014), and small ( $\leq 6$  mm) solid nodule number (0.008). The number of upper-lobe nodules and the number of solid nodules of a small size were the individual features that contributed most to the model and correlated best with OS among all categories of AI-detected nodule numbers.

### Survival tree analyses

A tree-based model incorporating AI-detected TNNs and the 8<sup>th</sup> edition of AJCC prognostic groups was constructed based on the best determination of OS for the entire cohort (Figure 5A). We found that the discrimination of survival curves for sub-stages was unsatisfactory with the current staging system in our study, especially in the sub-stages of IA2 to IB (IA2 *vs.* IA3: log-rank  $P=0.177$ ; IA3 *vs.* IB: log-rank  $P=0.778$ ) and IIA to IIB (log-rank  $P=0.236$ ). Moreover, in the stage III cohort, rather than using the traditional IIIA and IIIB classifications, the model grouped OS according to AI-detected TNNs (lower *vs.* higher: log-rank  $P<0.001$ ) since it showed a more effective determination of survival rates. The Kaplan-Meier curves of OS from the tree-based grouping scheme are shown in Figure 5B.

### Treatment failure analyses

To evaluate the potential relationship between AI-detected TNNs and tumor recurrence patterns, we further divided the stage III cohort into 2 groups depending on their first disease progression site. Among all 263 participants in the stage III group, 60 had local recurrence, 40 had distant metastasis, and 19 had progressive cancer without a specified pattern. Participants with localized recurrence had a lower AI-detected TNN (median: 14; IQR, 7.75 to 18.25)

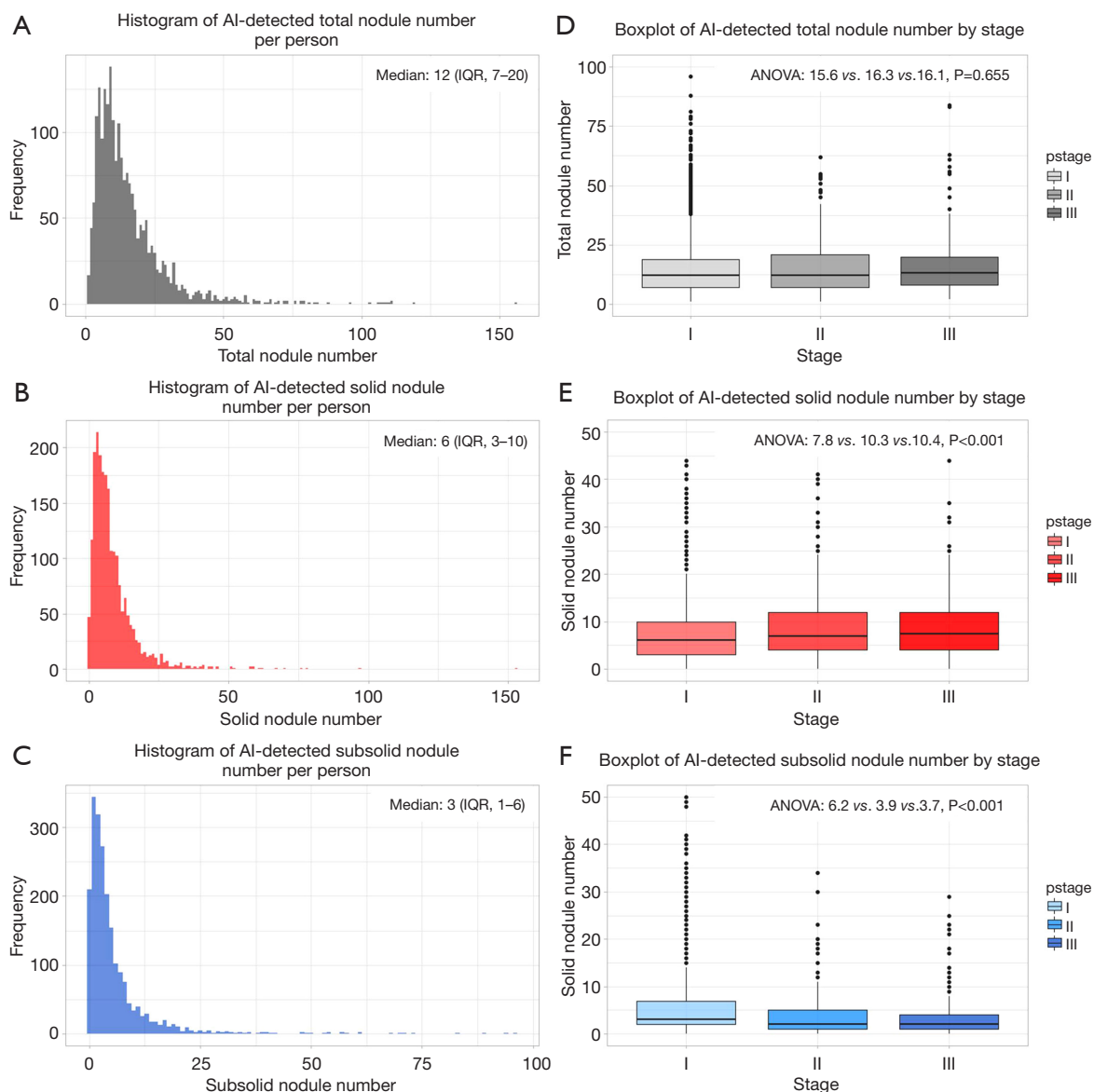


**Figure 2** Frequency distribution of the AI-detected nodules. (A) TNN, (B) solid nodule number, (C) subsolid nodule number, (D) TNN stratified by pathological stage, (E) solid nodule number stratified by pathological stage, (F) subsolid nodule number stratified by pathological stage. AI, artificial intelligence; TNN, total nodule number; IQR, interquartile range; ANOVA, analysis of variance.

compared with the distant metastasis group (median: 17; IQR, 10.75 to 23.25). However, the difference between these 2 groups was not statistically significant (Wilcoxon rank-sum  $P=0.077$ , Figure S4).

## Discussion

The widespread application of AI algorithms in PN detection is reshaping our knowledge on this topic. The

number of patients with tens or even hundreds of PNs is rapidly increasing. However, the interpretation of these lesions and their impact on surgical decision-making remain complicated and underrepresented. As the number of nodules grows, accurate diagnosis for every single nodule becomes onerous and statistically challenging. As an alternative, we hypothesized that TNN measured by a deep-learning algorithm may serve as a surrogate indicator of the probability of malignancy and metastasis in locally

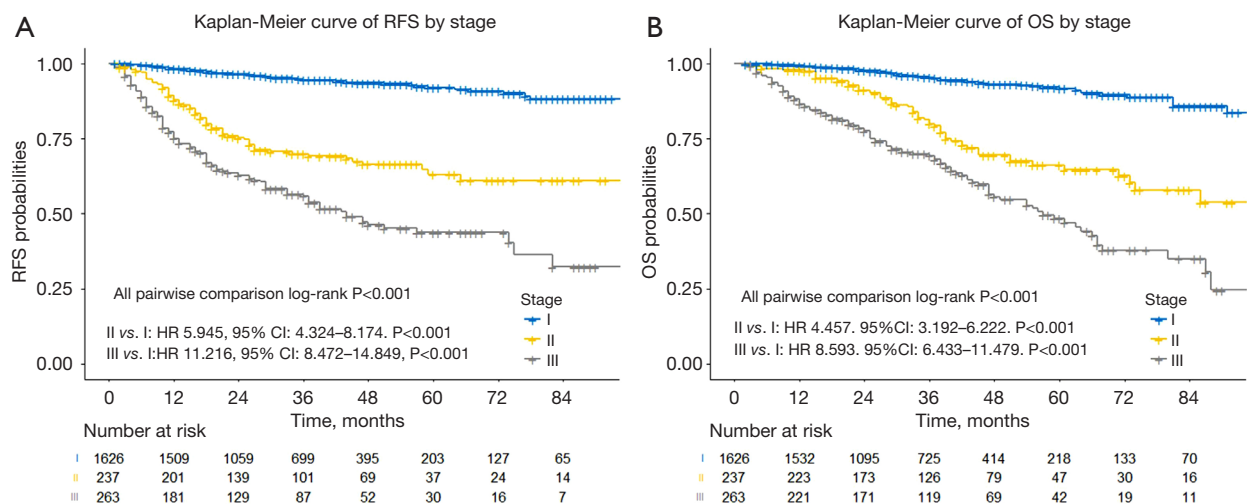


**Figure 3** Kaplan-Meier curves showing survival by stage in entire cohort. (A) RFS, (B) OS. Comparisons were conducted using a log-rank test. RFS, recurrence-free survival; OS, overall survival; CI, confidence interval; HR, hazard ratio.

advanced NSCLC. This hypothesis was preliminarily supported by our results, which showed that the TNN is an independent prognostic factor in stage III lung cancer.

The accurate measurement of TNNs is highly challenging. First, the definition of PN varies among radiologists and surgeons due to their different purposes: some may only report guideline-mandated PNs in order not to provoke panic in patients, while others may report all detected PNs for more accurate surgical planning. Unfortunately, both standards are rather subjective and have poor replicability. Second, the accuracy and robustness of a single radiologist or surgeon are limited. The sensitivity of PN detection by a single radiologist is around 77%, though this can be increased to 90% with a concurrent radiologist's help (32). However, such a method is time-consuming and remains subject to human error.

The emergence of a deep learning-based AI algorithm ensures the objectiveness and robustness of PN detection and, consequently, the measurement of TNNs. Mature algorithms have reached a diagnostic sensitivity of 85–100% (33–35). The best-performing deep learning algorithm is the LUNA16 challenge, which is based on the Lung Image Database Consortium and Image Database Resource Initiative (LIDC-IDRI) dataset and has exhibited an excellent sensitivity of over 95% with a less than 1.0 false positive per scan (36). The algorithm (InferRead CT Lung, InferVision) in this study was trained using over 350,000 chest CTs labeled by radiologists (20). In real-world applications, the performance of this model has

reached an area under the curve (AUC) of 0.89 in PN detection and can significantly improve the performance of radiologists (20–22). Our result showed the median TNN to be 12 per patient, much higher than the median of 2 per patient reported in the malignant cohort of the NELSON study (29). Such a difference may, on the one hand, be due to differences in CT radiation dosage, or on the other hand, may reflect differences in diagnostic preference and consistency between AI and human radiologists.

From a clinical standpoint, our results suggested that the TNN may be a simplified representation of the tumor burden in stage III NSCLC. In contrast to the results of the NELSON study, which showed that a higher nodule count favored a benign diagnosis (29), our study focused on more advanced NSCLC patients instead of a high-risk screening population. Past evidence vaguely showed that with confirmed histology, extensive nodal or systemic metastases are substantial evidence that multiple PNs indicate IPM (37), suggesting that a high TNN may relate to a higher pretest probability of IPM. Our results further supported this speculation by revealing the improved survival rates of the lower TNN group compared to the higher TNN group, which existed when analyzing the TNN as either a continuous or a binary variable, and thus strengthened our hypothesis.

It is worth noting that the factor that most impacted survival was the number of solid nodules, not the number of GGNs. For the GGN components, the International Association for the Study of Lung Cancer (IASLC)



**Table 3** Univariate and multivariate analyses of RFS stratified by stage

Variables	Univariate analysis			Multivariate analysis		
	HR	95% CI	P value	HR	95% CI	P value
Stage I (n=1,626, event =83)						
TNN (per 1 nodule increased)	1.010	0.998–1.022	0.102	1.007	0.994–1.020	0.292
Age (per 1 year increased)	1.034	1.012–1.057	0.002*	1.016	0.994–1.039	0.156
Female gender	0.650	0.422–0.999	0.050*	1.088	0.613–1.933	0.773
Positive smoking history	2.038	1.319–3.149	0.001*	1.155	0.632–2.111	0.639
Comorbid conditions	1.302	0.829–2.046	0.252			
Non-VATS approach	3.280	1.483–7.256	0.003*	1.814	0.805–4.087	0.151
Non-sublobar resection	1.861	1.087–3.186	0.024*	1.027	0.585–1.803	0.926
Non-adenocarcinoma	3.459	2.155–5.553	<0.001*	2.217	1.271–3.866	0.005*
Postoperative complications	0.901	0.284–2.862	0.860			
Adjuvant therapy	2.309	1.325–4.025	0.003*	1.409	0.780–2.545	0.256
AJCC stage IA2 (8th edition)	5.868	1.743–19.750	0.004*	4.497	1.306–15.486	0.017*
AJCC stage IA3 (8th edition)	11.566	3.448–38.790	<0.001*	7.719	2.202–27.065	0.001
AJCC stage IB (8th edition)	13.864	4.272–44.990	<0.001*	8.504	2.466–29.325	<0.001*
Stage II (n=237, event =70)						
TNN (per 1 nodule increased)	1.000	0.988–1.013	0.973	1.001	0.987–1.015	0.880
Age (per 1 year increased)	1.031	1.004–1.058	0.022*	1.030	1.002–1.059	0.034*
Female sex	1.504	0.924–2.449	0.100*	1.588	0.966–2.611	0.068
Positive smoking history	0.866	0.541–1.387	0.549			
Comorbid conditions	1.545	0.941–2.536	0.085*	1.274	0.758–2.139	0.361
Non-VATS approach	1.393	0.820–2.367	0.220			
Non-sublobar resection	0.871	0.273–2.776	0.816			
Non-adenocarcinoma	0.785	0.487–1.267	0.322			
Postoperative complications	0.420	0.058–3.023	0.389			
Adjuvant therapy	1.038	0.637–1.693	0.881			
AJCC stage IIB (8th edition)	0.837	0.484–1.445	0.523			
Stage III (n=263, event =119)						
TNN (per 1 nodule increased)	1.015	1.005–1.024	0.003*	1.012	1.002–1.022	0.021*
Age (per 1 year increased)	1.022	1.004–1.041	0.019*	1.019	1.000–1.039	0.051
Female sex	1.062	0.734–1.535	0.751			
Positive smoking history	1.013	0.707–1.452	0.942			
Comorbid conditions	0.862	0.600–1.238	0.421			
Non-VATS approach	1.574	1.029–2.407	0.036*	1.700	1.105–2.614	0.016*
Non-sublobar resection	0.835	0.367–1.902	0.668			
Non-adenocarcinoma	0.958	0.646–1.422	0.832			
Postoperative complications	1.425	0.718–2.828	0.311			
Adjuvant therapy	0.694	0.467–1.031	0.070*	0.812	0.539–1.224	0.319
AJCC stage IIIB (8th edition)	1.421	0.912–2.215	0.121			

\*, statistical significance. RFS, recurrence-free survival; HR, hazard ratio; CI, confidence interval; TNN, total nodule number; VATS, video-assisted thoracoscopic surgery; AJCC, American Joint Committee on Cancer.

**Table 4** Univariate and multivariate analyses of OS stratified by stage

Variables	Univariate analysis			Multivariate analysis		
	HR	95% CI	P value	HR	95% CI	P value
Stage I (n=1,626, event =80)						
TNN (per 1 nodule increased)	1.003	0.989–1.017	0.689	0.995	0.978–1.012	0.572
Age (per 1 year increased)	1.080	1.054–1.106	<0.001*	1.062	1.035–1.090	<0.001*
Female gender	0.381	0.241–0.603	<0.001*	0.722	0.403–1.295	0.274
Positive smoking history	2.634	1.697–4.090	<0.001*	1.259	0.705–2.250	0.436
Comorbid conditions	1.883	1.152–3.077	0.012*	1.182	0.713–1.962	0.517
Non-VATS approach	3.415	1.656–7.043	<0.001*	2.163	1.028–4.553	0.042*
Non-sublobar resection	1.232	0.737–2.059	0.427			
Non-adenocarcinoma	3.921	2.472–6.220	<0.001*	1.990	1.173–3.375	0.011*
Postoperative complications	1.155	0.418–3.191	0.782			
Adjuvant therapy	1.044	0.531–2.052	0.900			
AJCC stage IA2 (8th edition)	9.332	2.199–39.600	0.002*	5.510	1.285–23.633	0.022*
AJCC stage IA3 (8th edition)	14.513	3.389–62.150	<0.001*	6.554	1.494–28.743	0.013*
AJCC stage IB (8th edition)	14.918	3.575–62.240	<0.001*	6.839	1.606–29.127	0.009*
Stage II (n=237, event =61)						
TNN (per 1 nodule increased)	1.000	0.989–1.012	0.965	1.001	0.988–1.013	0.934
Age (per 1 year increased)	1.044	1.015–1.074	0.003*	1.044	1.015–1.074	0.003*
Female sex	1.275	0.737–2.209	0.385			
Positive smoking history	1.138	0.678–1.909	0.625			
Comorbid conditions	1.394	0.831–2.339	0.208			
Non-VATS approach	1.327	0.763–2.309	0.317			
Non-sublobar resection	0.601	0.187–1.929	0.392			
Non-adenocarcinoma	1.105	0.668–1.827	0.699			
Postoperative complications	0.496	0.069–3.587	0.488			
Adjuvant therapy	0.723	0.436–1.201	0.210			
AJCC stage IIB (8th edition)	0.700	0.395–1.240	0.222			
Stage III (n=263, event =108)						
TNN (per 1 nodule increased)	1.018	1.008–1.029	<0.001*	1.013	1.002–1.025	0.021*
Age (per 1 year increased)	1.035	1.015–1.056	<0.001*	1.036	1.014–1.058	<0.001*
Female sex	0.645	0.428–0.972	0.036*	1.054	0.568–1.955	0.868
Positive smoking history	1.716	1.168–2.521	0.006*	1.443	0.792–2.631	0.231
Comorbid conditions	0.826	0.565–1.209	0.325			
Non-VATS approach	2.340	1.556–3.517	<0.001*	2.480	1.541–3.990	<0.001*
Non-sublobar resection	0.724	0.293–1.789	0.483			
Non-adenocarcinoma	1.614	1.093–2.384	0.016*	0.933	0.567–1.535	0.784
Postoperative complications	1.380	0.690–2.761	0.362			
Adjuvant therapy	0.458	0.309–0.679	<0.001*	0.560	0.394–0.913	0.017*
AJCC stage IIIB (8th edition)	1.841	1.176–2.882	0.008*	1.338	0.823–2.175	0.241

\*, statistical significance. OS, overall survival; HR, hazard ratio; CI, confidence interval; TNN, total nodule number; VATS, video-assisted thoracoscopic surgery; AJCC, American Joint Committee on Cancer.

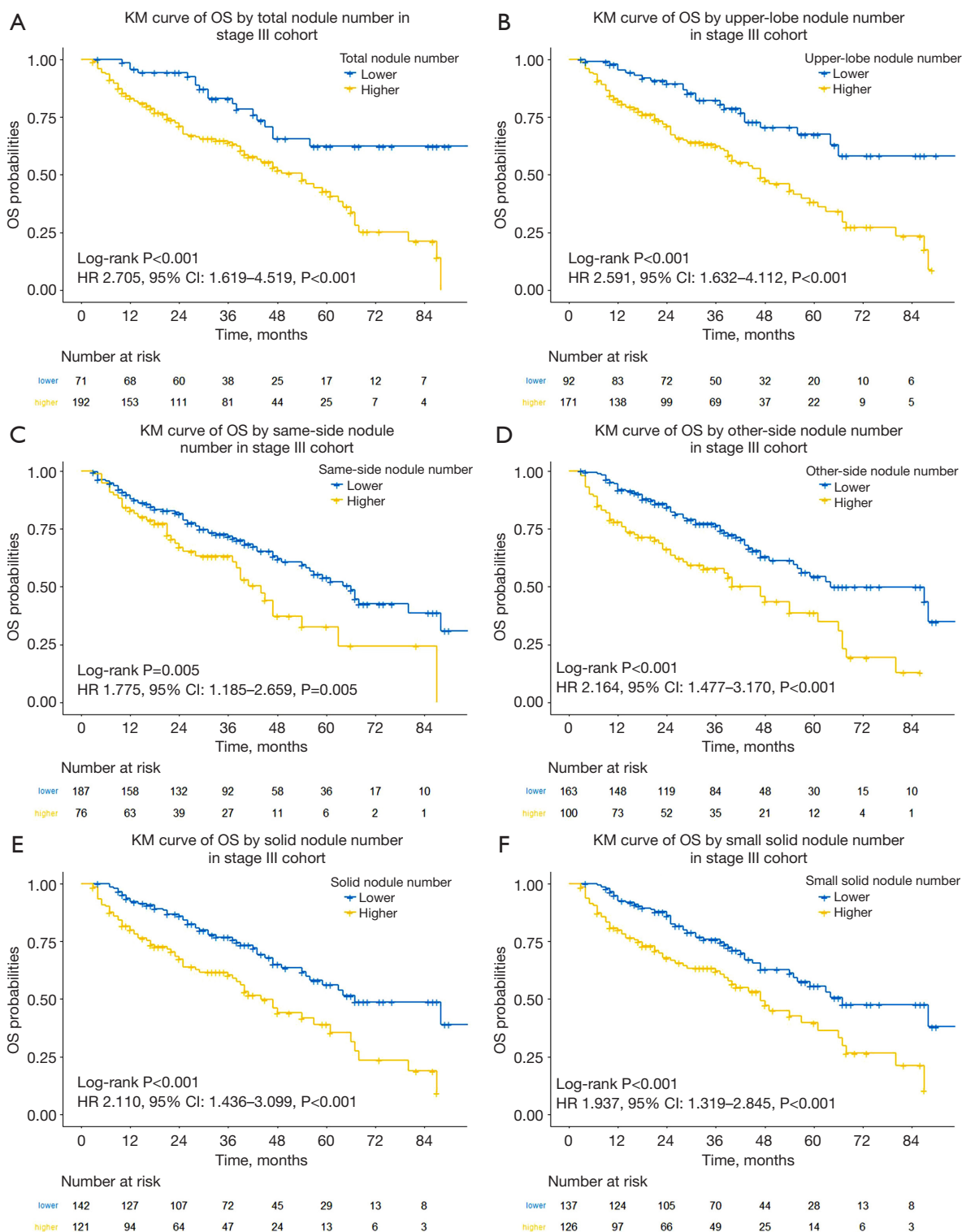


**Figure 4** Kaplan-Meier curves showing OS by AI-detected nodule number in the stage III cohort. (A) TNN, (B) upper-lobe nodule number, (C) same-side nodule number, (D) other-side nodule number, (E) solid nodule number, (F) small ( $\leq 6$  mm) solid nodule number. Comparisons were conducted using a log-rank test. AI, artificial intelligence; TNN, total nodule number; OS, overall survival; HR, hazard ratio; CI, confidence interval.

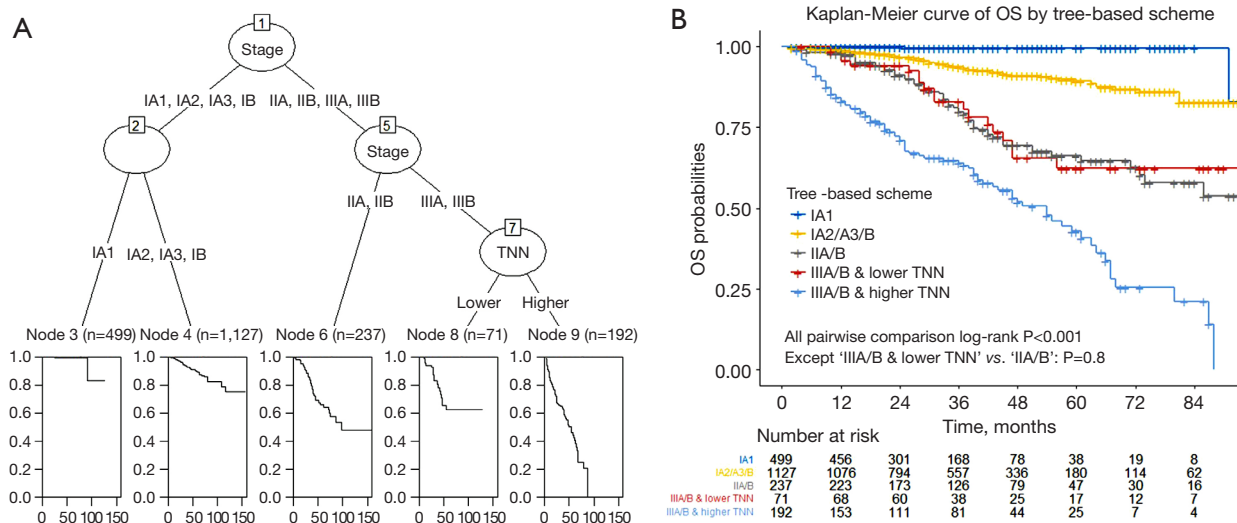


**Figure 5** Survival tree analysis. (A) Recursive partitioning-generated survival tree based on the best determination of OS using AI-detected TNNs and the 8<sup>th</sup> edition of AJCC stage. Both the TNN and stage were modeled as categorical variables. (B) Kaplan-Meier curves showing OS by tree-based scheme in the entire cohort. Comparisons were conducted using a log-rank test. OS, overall survival; AI, artificial intelligence; AJCC, American Joint Committee on Cancer; TNN, total nodule number.

guidelines suggest that the prognosis with multifocal GGNs be similar to that of a single minimally invasive adenocarcinoma (MIA) or adenocarcinoma in situ (AIS) (38), while others have indicated that there are metastatic GGNs on a molecular level (39). In our study, concurrent multiple GGNs in all 3 stages did not increase HR, indicating that concurrent multiple GGNs in invasive lung cancer possess the same biological behavior as in multifocal GGN cases. For solid components, most of the nodules were  $\leq 6$  mm and radiologically benign, with a round shape, no spiculation, and no lobulation. However, the growth of a few unresected nodules suggested their malignancy (Figure S5). These results showed that diagnosis using traditional radiological characteristics for multiple PNs in stage III NSCLC patients is not that reliable. Treatment failure pattern analysis showed that a higher TNN was related to distant metastasis (without statistical significance due to small sample size), indicating that TNN was not only an indicator of IPM, but also a visual representation of the systematic tumor burden.

From a surgeon's perspective, the impact of PNs on surgical planning is substantial. Convincing a patient to accept unresected GGNs after surgery is difficult even with the guidelines' support. A sublobar resection of a GGN may turn into a lobectomy due to multiple GGNs being detected by AI, while a lobectomy may also be changed to a

sublobar resection due to bilateral nodules being clinically diagnosed as a separate primary lung cancer. However, no prior research has shown the validity of such an approach. Our study provided the first proof of concept that the TNN, determined by deep learning algorithms, should be considered a mandatory test before surgical planning. It would be reasonable for surgeons to be more aggressive in the resection of solid nodules instead of GGNs. Moreover, neoadjuvant therapy should be considered for stage III patients with a higher TNN for better PN evaluation since empirical diagnosis may not be reliable.

Some may argue that positron emission tomography-computed tomography (PET-CT) is a valid method for differentiating MPLC and IPM before surgery. However, the partial-volume effect of PET-CT prevents it from achieving optimum diagnostic performance for solid nodules of less than 8 mm, which represented 85.6% of the solid nodules in our study (26,40,41). Moreover, PET-CT is relatively expensive for most underdeveloped countries and not affordable for every patient.

As a retrospective study, our results need validation before clinical application. However, no public databases currently provide sufficient data. Therefore, prospective validation is necessary yet time-consuming. The AI algorithm requires optimization to further reduce the false positive rate, and perivascular nodule detection still

needs improvement. Technological developments for the alignment of pre- and postoperative PNs on chest CT are urgently needed. The goals of future research are to analyze the growth speed and pathology findings of the unresected PNs and investigate the biological nature of the TNN, especially in the stage III NSCLC cohort. To our knowledge, this study was the first to identify that TNN measured by a deep learning algorithm is an independent prognostic factor in stage III lung cancer. Our results suggested a potentially critical clinical application of AI as a mandatory examination for surgical decision-making. The current cutoff point of the TNN is still preliminary but shows great potential and provides motivation for future validation.

### Acknowledgments

We would like to thank Yuqing Huang, Xianjun Min, and Guotian Pei from the Beijing Haidian Hospital for sharing their thoughts on this work. We would like to thank Yutong Wang from the University of Michigan for his help in polishing our paper.

*Funding:* This work was supported by the National Natural Science Foundation of China (82002983, XC).

### Footnote

*Reporting Checklist:* Available at <https://atm.amegroups.com/article/view/10.21037/atm-21-3231/rc>

*Data Sharing Statement:* Available at <https://atm.amegroups.com/article/view/10.21037/atm-21-3231/ds>

*Peer Review File:* Available at <https://atm.amegroups.com/article/view/10.21037/atm-21-3231/prf>

*Conflicts of Interest:* All authors have completed the ICMJE uniform disclosure form (available at <https://atm.amegroups.com/article/view/10.21037/atm-21-3231/coif>). XC reports funding from the National Natural Science Foundation of China (82002983). DW, JS, and WT were employed by the company Beijing Infervision Technology Co., Ltd. The other authors have no conflicts of interest to declare.

*Ethical Statement:* The authors are accountable for all aspects of the work in ensuring that questions related to the accuracy or integrity of any part of the work

are appropriately investigated and resolved. The study was conducted in accordance with the Declaration of Helsinki (as revised in 2013). The study involving human participants was reviewed and approved by the Institutional Review Board of Peking University People's Hospital (2020PHB385-01). Individual consent for this de-identified retrospective analysis was waived.

*Open Access Statement:* This is an Open Access article distributed in accordance with the Creative Commons Attribution-NonCommercial-NoDerivs 4.0 International License (CC BY-NC-ND 4.0), which permits the non-commercial replication and distribution of the article with the strict proviso that no changes or edits are made and the original work is properly cited (including links to both the formal publication through the relevant DOI and the license). See: <https://creativecommons.org/licenses/by-nc-nd/4.0/>.

### References

1. Bray F, Ferlay J, Soerjomataram I, et al. Global cancer statistics 2018: GLOBOCAN estimates of incidence and mortality worldwide for 36 cancers in 185 countries. *CA Cancer J Clin* 2018;68:394-424.
2. National Lung Screening Trial Research Team; Aberle DR, Adams AM, et al. Reduced lung-cancer mortality with low-dose computed tomographic screening. *N Engl J Med* 2011;365:395-409.
3. Detterbeck FC, Mazzone PJ, Naidich DP, et al. Screening for lung cancer: Diagnosis and management of lung cancer, 3rd ed: American College of Chest Physicians evidence-based clinical practice guidelines. *Chest* 2013;143:e78S-92S.
4. Ruparel M, Quaife SL, Navani N, et al. Pulmonary nodules and CT screening: the past, present and future. *Thorax* 2016;71:367-75.
5. Smith RA, Andrews KS, Brooks D, et al. Cancer screening in the United States, 2017: A review of current American Cancer Society guidelines and current issues in cancer screening. *CA Cancer J Clin* 2017;67:100-21.
6. Wood DE, Kazerooni EA, Baum SL, et al. Lung Cancer Screening, Version 3.2018, NCCN Clinical Practice Guidelines in Oncology. *J Natl Compr Canc Netw* 2018;16:412-41.
7. de Koning HJ, van der Aalst CM, de Jong PA, et al. Reduced Lung-Cancer Mortality with Volume CT Screening in a Randomized Trial. *N Engl J Med* 2020;382:503-13.
8. Gould MK, Tang T, Liu IL, et al. Recent Trends in the

- Identification of Incidental Pulmonary Nodules. *Am J Respir Crit Care Med* 2015;192:1208-14.
9. Erickson BJ, Korfiatis P, Akkus Z, et al. Machine Learning for Medical Imaging. *Radiographics* 2017;37:505-15.
  10. Armato SG 3rd, Altman MB, La Rivière PJ. Automated detection of lung nodules in CT scans: effect of image reconstruction algorithm. *Med Phys* 2003;30:461-72.
  11. Hwang EJ, Park CM. Clinical Implementation of Deep Learning in Thoracic Radiology: Potential Applications and Challenges. *Korean J Radiol* 2020;21:511-25.
  12. Ather S, Kadir T, Gleeson F. Artificial intelligence and radiomics in pulmonary nodule management: current status and future applications. *Clin Radiol* 2020;75:13-9.
  13. Murphy A, Skalski M, Gaillard F. The utilisation of convolutional neural networks in detecting pulmonary nodules: a review. *Br J Radiol* 2018;91:20180028.
  14. Hua KL, Hsu CH, Hidayati SC, et al. Computer-aided classification of lung nodules on computed tomography images via deep learning technique. *Onco Targets Ther* 2015;8:2015-22.
  15. Cheng JZ, Ni D, Chou YH, et al. Computer-Aided Diagnosis with Deep Learning Architecture: Applications to Breast Lesions in US Images and Pulmonary Nodules in CT Scans. *Sci Rep* 2016;6:24454.
  16. Li W, Cao P, Zhao D, et al. Pulmonary Nodule Classification with Deep Convolutional Neural Networks on Computed Tomography Images. *Comput Math Methods Med* 2016;2016:6215085.
  17. Liu S, Xie Y, Jirapatnakul A, et al. Pulmonary nodule classification in lung cancer screening with three-dimensional convolutional neural networks. *J Med Imaging (Bellingham)* 2017;4:041308.
  18. da Silva GLF, Valente TLA, Silva AC, et al. Convolutional neural network-based PSO for lung nodule false positive reduction on CT images. *Comput Methods Programs Biomed* 2018;162:109-18.
  19. Xie Y, Xia Y, Zhang J, et al. Knowledge-based Collaborative Deep Learning for Benign-Malignant Lung Nodule Classification on Chest CT. *IEEE Trans Med Imaging* 2019;38:991-1004.
  20. Wang Y, Yan F, Lu X, et al. IILS: Intelligent imaging layout system for automatic imaging report standardization and intra-interdisciplinary clinical workflow optimization. *EBioMedicine* 2019;44:162-81.
  21. Liu K, Li Q, Ma J, et al. Evaluating a Fully Automated Pulmonary Nodule Detection Approach and Its Impact on Radiologist Performance. *Radiology: Artificial Intelligence* 2019;1.
  22. Yang F, Fan J, Tian Z, et al. Population-based research of pulmonary subsolid nodule CT screening and artificial intelligence application. *Chin J Thorac Cardiovasc Surg* 2020;36:145-50.
  23. McWilliams A, Tammemagi MC, Mayo JR, et al. Probability of cancer in pulmonary nodules detected on first screening CT. *N Engl J Med* 2013;369:910-9.
  24. Horeweg N, van Rosmalen J, Heuvelmans MA, et al. Lung cancer probability in patients with CT-detected pulmonary nodules: a prespecified analysis of data from the NELSON trial of low-dose CT screening. *Lancet Oncol* 2014;15:1332-41.
  25. Walter JE, Heuvelmans MA, de Jong PA, et al. Occurrence and lung cancer probability of new solid nodules at incidence screening with low-dose CT: analysis of data from the randomised, controlled NELSON trial. *Lancet Oncol* 2016;17:907-16.
  26. Gould MK, Donington J, Lynch WR, et al. Evaluation of individuals with pulmonary nodules: when is it lung cancer? Diagnosis and management of lung cancer, 3rd ed: American College of Chest Physicians evidence-based clinical practice guidelines. *Chest* 2013;143:e93S-e120S.
  27. Callister ME, Baldwin DR, Akram AR, et al. British Thoracic Society guidelines for the investigation and management of pulmonary nodules. *Thorax* 2015;70 Suppl 2:ii1-ii54.
  28. MacMahon H, Naidich DP, Goo JM, et al. Guidelines for Management of Incidental Pulmonary Nodules Detected on CT Images: From the Fleischner Society 2017. *Radiology* 2017;284:228-43.
  29. Heuvelmans MA, Walter JE, Peters RB, et al. Relationship between nodule count and lung cancer probability in baseline CT lung cancer screening: The NELSON study. *Lung Cancer* 2017;113:45-50.
  30. Walter JE, Heuvelmans MA, de Bock GH, et al. Relationship between the number of new nodules and lung cancer probability in incidence screening rounds of CT lung cancer screening: The NELSON study. *Lung Cancer* 2018;125:103-8.
  31. Girard N, Deshpande C, Lau C, et al. Comprehensive histologic assessment helps to differentiate multiple lung primary nonsmall cell carcinomas from metastases. *Am J Surg Pathol* 2009;33:1752-64.
  32. Nair A, Sreaton NJ, Holemans JA, et al. The impact of trained radiographers as concurrent readers on performance and reading time of experienced radiologists in the UK Lung Cancer Screening (UKLS) trial. *Eur Radiol* 2018;28:226-34.
  33. Setio AA, Ciampi F, Litjens G, et al. Pulmonary Nodule

- Detection in CT Images: False Positive Reduction Using Multi-View Convolutional Networks. *IEEE Trans Med Imaging* 2016;35:1160-9.
34. Dou Q, Chen H, Yu L, et al. Multilevel Contextual 3-D CNNs for False Positive Reduction in Pulmonary Nodule Detection. *IEEE Trans Biomed Eng* 2017;64:1558-67.
  35. Tajbakhsh N, Suzuki K. Comparing two classes of end-to-end machine-learning models in lung nodule detection and classification: MTANNs vs. CNNs. *Pattern Recognition* 2017;63:476-486.
  36. Setio AAA, Traverso A, de Bel T, et al. Validation, comparison, and combination of algorithms for automatic detection of pulmonary nodules in computed tomography images: The LUNA16 challenge. *Med Image Anal* 2017;42:1-13.
  37. Dettnerbeck FC, Nicholson AG, Franklin WA, et al. The IASLC Lung Cancer Staging Project: Summary of Proposals for Revisions of the Classification of Lung Cancers with Multiple Pulmonary Sites of Involvement in the Forthcoming Eighth Edition of the TNM Classification. *J Thorac Oncol* 2016;11:639-50.
  38. Dettnerbeck FC, Marom EM, Arenberg DA, et al. The IASLC Lung Cancer Staging Project: Background Data and Proposals for the Application of TNM Staging Rules to Lung Cancer Presenting as Multiple Nodules with Ground Glass or Lepidic Features or a Pneumonic Type of Involvement in the Forthcoming Eighth Edition of the TNM Classification. *J Thorac Oncol* 2016;11:666-80.
  39. Li R, Li X, Xue R, et al. Early metastasis detected in patients with multifocal pulmonary ground-glass opacities (GGOs). *Thorax* 2018;73:290-2.
  40. Soret M, Bacharach SL, Buvat I. Partial-volume effect in PET tumor imaging. *J Nucl Med* 2007;48:932-45.
  41. Groheux D, Quere G, Blanc E, et al. FDG PET-CT for solitary pulmonary nodule and lung cancer: Literature review. *Diagn Interv Imaging* 2016;97:1003-17.
- (English Language Editors: L. Roberts and J. Jones)

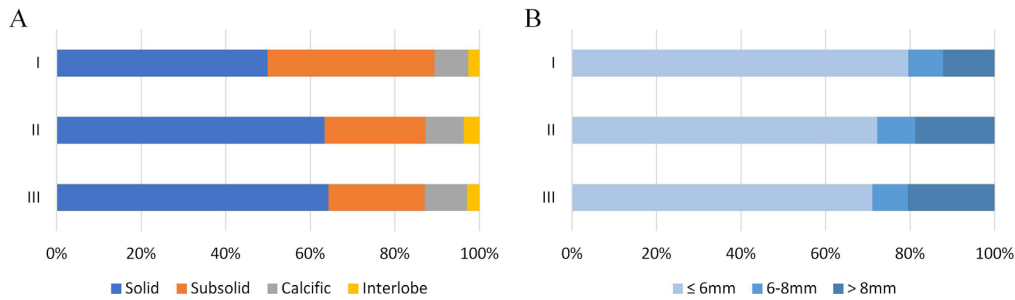
**Cite this article as:** Chen X, Qi Q, Sun Z, Wang D, Sun J, Tan W, Liu X, Liu T, Hong N, Yang F. Total nodule number as an independent prognostic factor in resected stage III non-small cell lung cancer: a deep learning-powered study. *Ann Transl Med* 2022;10(2):33. doi: 10.21037/atm-21-3231

Table S1 Univariate and multivariate survival analyses of entire cohort

Variables	Univariate Analysis			Multivariate Analysis		
	HR	95% CI	P Value	HR	95% CI	P Value
Recurrence-free survival (RFS)						
TNN (per 1 nodule increased)	1.008	1.001-1.014	0.017*	1.006	0.999-1.012	0.080
Age (per 1 year increased)	1.027	1.015-1.039	<0.001*	1.033	1.019-1.046	<0.001*
Sex						
Male	Reference			Reference		
Female	0.625	0.491-0.795	<0.001*	1.249	0.884-1.765	0.207
Smoking History						
No	Reference			Reference		
Yes	1.931	1.521-2.451	<0.001*	1.157	0.817-1.637	0.412
Comorbid Conditions						
No	Reference					
Yes	1.098	0.860-1.401	0.453			
Surgical Approach						
VATS	Reference			Reference		
Non-VATS	1.369	2.910-5.313	<0.001*	1.521	1.086-2.130	0.015*
Surgical Procedure						
Sublobar Resection	Reference			Reference		
Non-Sublobar Resection	3.601	2.401-5.400	<0.001*	1.516	0.983-2.338	0.060
Histologic Type						
Adenocarcinoma	Reference			Reference		
Non-Adenocarcinoma	2.416	1.872-3.117	<0.001*	1.070	0.773-1.482	0.682
Postoperative Complications						
No	Reference					
Yes	1.225	0.701-2.139	0.476			
Adjuvant Therapy						
No	Reference			Reference		
Yes	4.162	3.277-5.287	<0.001*	1.330	0.987-1.793	0.061
AJCC 8th edition, T stage						
T1	Reference			Reference		
T2	3.449	2.602-4.573	<0.001*	1.781	1.304-2.431	<0.001*
T3	8.036	5.603-11.525	<0.001*	3.568	2.386-5.334	<0.001*
T4	10.735	6.571-17.537	<0.001*	3.861	2.245-6.641	<0.001*
AJCC 8th edition, N stage						
N0	Reference			Reference		
N1	4.988	3.570-6.969	<0.001*	2.852	1.941-4.190	<0.001*
N2	7.501	5.760-9.769	<0.001*	4.269	3.113-5.855	<0.001*
Overall survival (OS)						
TNN (per 1 nodule increased)	1.006	0.999-1.012	0.099	1.002	0.995-1.009	0.590
Age (per 1 year increased)	1.048	1.035-1.062	<0.001*	1.057	1.042-1.072	<0.001*
Sex						
Male	Reference			Reference		
Female	0.432	0.331-0.564	<0.001*	0.961	0.665-1.388	0.830
Smoking History						
No	Reference			Reference		
Yes	2.581	2.007-3.319	<0.001*	1.348	0.945-1.924	0.100
Comorbid Conditions						
No	Reference					
Yes	1.182	0.915-1.527	0.200			
Surgical Approach						
VATS	Reference			Reference		
Non-VATS	4.050	3.023-5.426	<0.001*	1.827	1.312-2.545	<0.001*
Surgical Procedure						
Sublobar Resection	Reference			Reference		
Non-Sublobar Resection	2.419	1.629-3.594	<0.001*	1.089	0.711-1.668	0.696
Histologic Type						
Adenocarcinoma	Reference			Reference		
Non-Adenocarcinoma	2.936	2.275-3.790	<0.001*	1.380	1.001-1.903	0.049*
Postoperative Complications						
No	Reference					
Yes	1.349	0.785-2.321	0.279			
Adjuvant Therapy						
No	Reference			Reference		
Yes	2.337	1.816-3.007	<0.001*	0.890	0.659-1.201	0.444
AJCC 8th edition, T stage						
T1	Reference			Reference		
T2	2.666	1.973-3.602	<0.001*	1.455	1.045-2.025	0.027*
T3	6.839	4.720-9.908	<0.001*	2.900	1.922-4.374	<0.001*
T4	11.987	7.548-19.037	<0.001*	4.537	2.700-7.623	<0.001*
AJCC 8th edition, N stage						
N0	Reference			Reference		
N1	3.621	2.536-5.171	<0.001*	2.632	1.772-3.910	<0.001*
N2	5.490	4.162-7.242	<0.001*	4.325	3.124-5.988	<0.001*

HR, hazard ratio; CI, confidence interval; TNN, total nodule number; VATS, video-assisted thoracoscopic surgery; AJCC, American Joint Committee on Cancer; \*, statistical significance.





**Figure S1** Bar chart showing the percentage of AI-detected nodule categories stratified by pathological stage. (A) nodule type, (B) solid nodule size. AI, artificial intelligence.

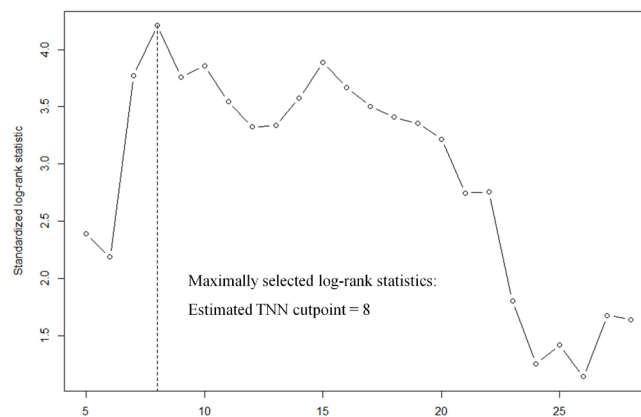


**Figure S2** Maximally selected log-rank statistics showing the optimal cutoff value of AI-detected TNN for predicting overall survival. The optimal cutoff value of 8 was selected. AI, artificial intelligence; TNN, total nodule number.

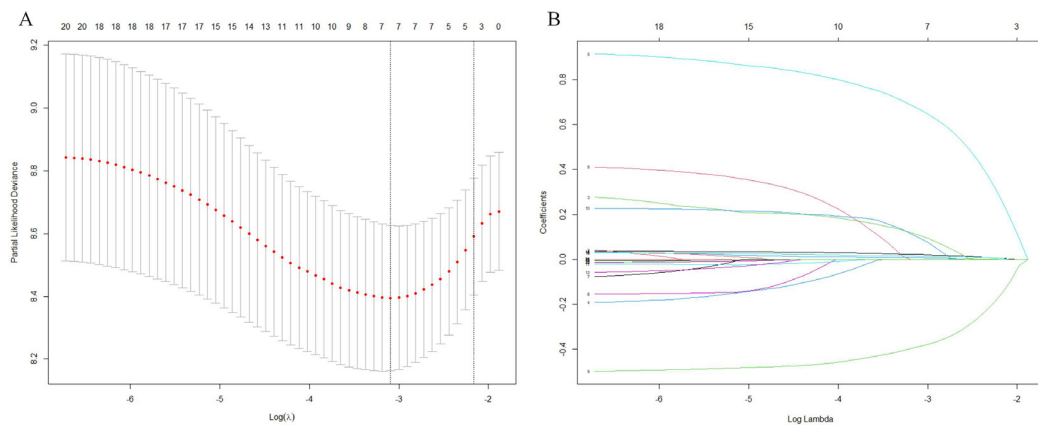


**Figure S3** Feature selection with LASSO. LASSO Cox regression model was built with both clinicopathologic characteristics and all categories of AI-detected nodule numbers (as continuous variables). (A) Red dots indicated average deviance values for each model with a given  $\lambda$ ; the dotted vertical lines were drawn at the optimal values by using the minimum mean square error (MSE) criteria. The optimal  $\lambda$  value of 0.0453 was selected. (B) The process of feature selection and resulting features with nonzero coefficients were indicated in the plot. LASSO, least absolute shrinkage and selection operator; AI, artificial intelligence.

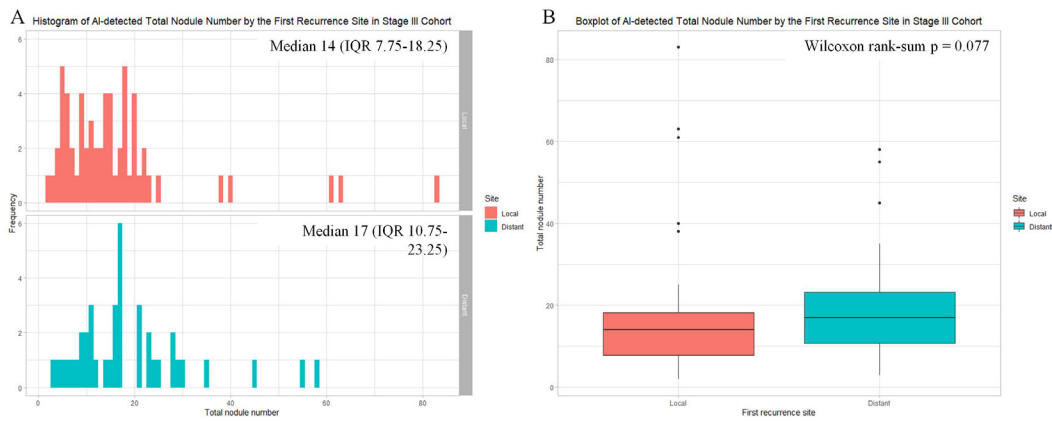


**Figure S4** AI-detected TNN stratified by recurrence pattern in stage III cohort. (A) histograms showing the frequency distribution, (B) boxplots showing the central tendency. AI, artificial intelligence; TNN, total nodule number; IQR, interquartile range.

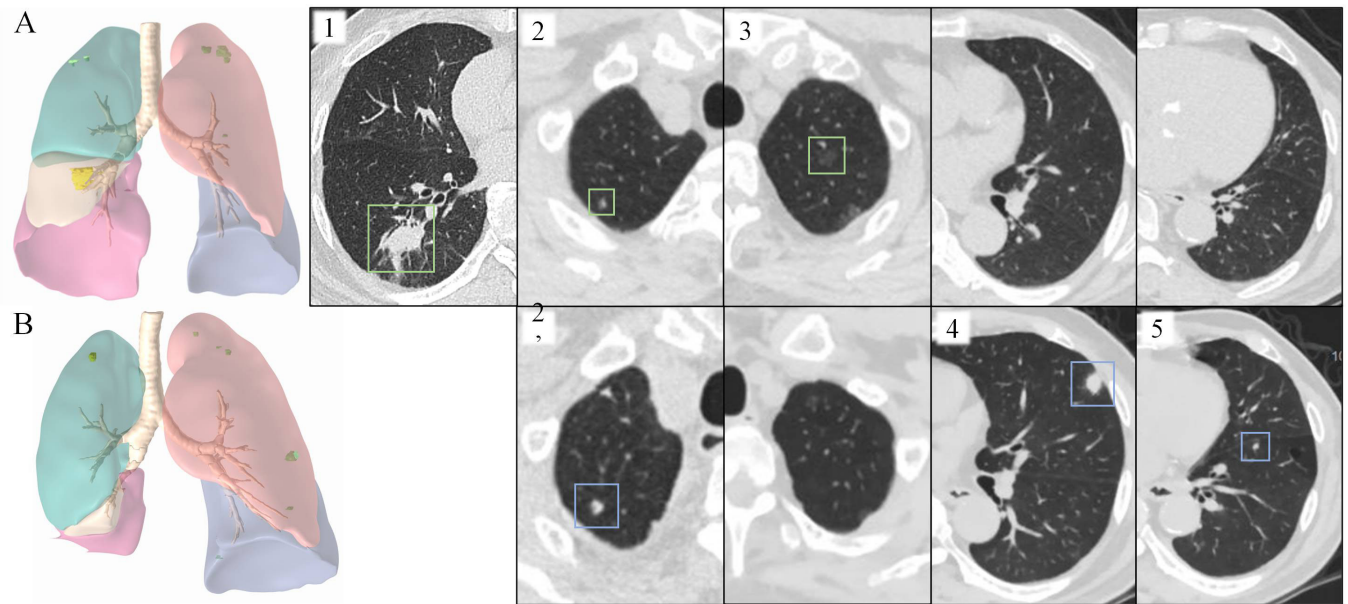


**Figure S5** A case report: 80-year-old male underwent right lower lobe lobectomy and diagnosed with pathologic stage IIIA lung adenocarcinoma. (A) Preoperative chest CT showed the primary tumor at right lower lobe (#1); a small solid nodule with benign-looking radiological features at right upper lobe (#2), which also exhibited no FDG uptake on PET-CT; and a pure GGN at left upper lobe (#3). (B) Postoperative follow-up chest CT showed the growth of right upper lobe nodule (#2 to #2'), which indicated its malignancy; and the occurrence of new solid nodules at left upper lobe (#4) and left lower lobe (#5), which suggested intrapulmonary metastases. CT, computed tomography; FDG, fluorodeoxyglucose; PET, positron emission tomography; GGN, ground-glass nodule.